

Joint fatigue-based optimal posture prediction for maximizing endurance time in box carrying task

Shuvrodeb Barman¹ · Yujiang Xiang¹ · Ritwik Rakshit² · James Yang²

Received: 25 November 2021 / Accepted: 20 May 2022 / Published online: 20 June 2022 © The Author(s), under exclusive licence to Springer Nature B.V. 2022

Abstract

In this study, the three-compartment controller fatigue model is integrated with an inverse dynamics optimization routine to predict the optimal posture, joint fatigue, and endurance time for a box carrying task. The two-dimensional human model employed has 10 degrees of freedom. For the box carrying task, the feet are fixed on the ground, and the hand location and box weight are given. In the joint fatigue-based posture prediction formulation, the design variables are joint angles, three-compartment control values, and total box carrying duration (endurance time). The objective is to maximize the total time subject to task and fatigue constraints, including compartment unity constraint, residual capacity constraint, and a novel coupled failure constraint. The optimization successfully predicts the optimal posture, joint torque, endurance time, joint fatigue progression, and joint failure conditions. The proposed novel joint fatigue-based formulation predicts the optimal posture for maximizing the endurance time with a given box weight for a box-carrying task. Finally, the simulation is computationally efficient, and the optimal results are achieved in about 5 seconds CPU time on a regular computer.

Keywords Fatigue prediction \cdot Endurance time prediction \cdot Posture prediction \cdot Box carrying \cdot Three-compartment controller fatigue model

1 Introduction

Joint fatigue associated with weight-carrying during manual material handling (MMH) tasks can prove to be a significant contributor to the loss of muscle force capacity. Since fatigue is the cumulative result of various physiological and neurological processes occurring simultaneously, it is very hard to single out the contribution of any one phenomenon making the task of computing fatigue-related force loss quite challenging [1, 3, 8]. Due to the variety of weights and carrying situations in the workplace in manufacturing, construction [5, 20], and healthcare industries [7], it is imperative to have a risk assessment tool that can routinely be

Y. Xiang yujiang.xiang@okstate.edu

Department of Mechanical Engineering, Texas Tech University, Lubbock, TX 79409, USA



School of Mechanical and Aerospace Engineering, Oklahoma State University, Stillwater, OK 74078, USA

used to determine factors, such as best posture, maximum weight capacity, and endurance time for the carrying task to minimize work-related injuries. Although physical prototypes are needed to develop new equipment or create new workspaces, predictive biomechanical human simulations can provide an efficient way to interact with the new environment. The optimization-based dynamic modeling and simulation method [28] coupled with muscle fatigue and recovery model [27] is a promising approach for predicting fatigue in box carrying tasks.

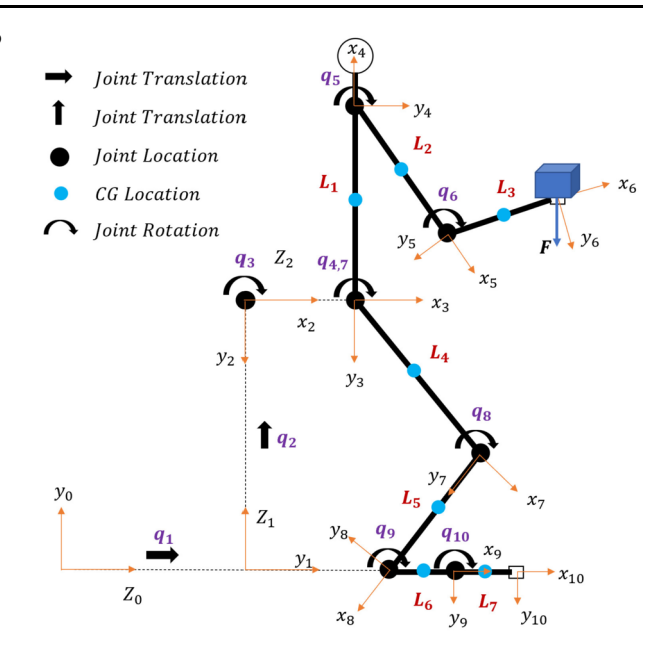
Kinematics- and physics-based posture prediction has previously been studied [14, 23, 26, 33, 34]. However, these studies only considered the final posture without considering holding the posture for a certain time, i.e., for a box-carrying task. In addition, they did not consider fatigue in the formulation. Optimization-based dynamic modeling is another well-established technique that helps determine the joint torques and forces required to complete a specific task [25, 31]. Inverse dynamics-based posture/motion predictions can provide the optimal posture/motion for any task, given a mathematically rigorous objective function and a set of constraints that mimic the actual working conditions and human limitations. To achieve this, a choice of formulations for the equations of motion (EOM) are available. The Lagrangian formulation uses 4×4 transformation matrices [28, 29], while the Newton-Euler method uses 3×3 rotation matrices for the dynamics calculation [2]. To find out the optimal results, a sequential quadratic programming (SQP) based non-linear optimizer can be used [19]. Though such an approach is indeed useful in posture and motion predictions, the effect of muscle fatigue on the task has not been integrated with this so far. This can lead to errors in prediction, thereby reducing the efficiency of the risk assessment tool being developed.

Fatigue models are mostly based upon analytical or experimental methods. While the experiment-based models have advanced [18, 22] since the pioneering work by Rohmert [24], those are typically applicable for simpler tasks. For more complex tasks, the inclusion of one or more decay terms [11, 13] into the existing analytical models can be useful at the single muscle level. However, these models cannot handle task-related factors like joint angles, which is imperative for optimal posture prediction. To solve this issue, a three-compartment controller (3CC) fatigue model, including resting, active and fatigued compartments, was proposed [27]. The relationship between these compartments are governed by three first-order differential equations. This model is consistent with muscle physiology and joint biomechanical properties and can handle complex biomechanical tasks.

Pereira et al. [21] did a pioneering work by applying a physics-based fatigue model to a single elbow joint. Since then, little advance has been made to analyze the task-specific fatigue results for complex biomechanical models. In this article, the three-compartment controller fatigue model will be integrated with a two-dimensional (2D) 10 degrees of freedom (DOFs) human model. The inverse dynamics optimization-based prediction method considering fatigue will be implemented to find the endurance time for a weight-carrying task. The joint torques are evaluated using recursive Lagrangian equations. In addition to determining the maximum endurance time when the task fails, the joints that cause the failure will also be identified using a novel coupled joint failure condition. It makes this research a benchmark study for further investigations of more complex tasks such as the repetitive lifting motion prediction considering fatigue. The contents of the article are organized as follows: Section 2 discusses the 2D human model and Denavit-Hartenberg (DH) parameters. Section 3 discusses the EOM and the 3CC fatigue model. Section 4 presents the optimization formulation. Section 5 presents the results obtained from the simulations and gives a detailed discussion, and Section 6 concludes this study with some closing remarks.



Fig. 1 A 2D human model setup for the carrying endurance time and fatigue status predictions



2 Human model

For the box carrying-fatigue simulation, a human model is defined in joint space with 10 DOFs. The first two DOFs (q_1, q_2) are global translation in the forward (z) and the upward (y) directions, and the third (q_3) is global clockwise rotation (β) . The global translations q_1 , q_2 and the rotation q_3 refer to the movements of the whole body at hip joint in the global reference frame. This can be better understood from the DH table in Table 1. The remaining seven DOFs correspond to the rotation movements-spine flexion (q_4) , shoulder flexion (q_5) , elbow extension (q_6) , hip extension (q_7) , knee flexion (q_8) , ankle plantar flexion (q_9) , and metatarsophalangeal extension (q_{10}) , respectively. The anthropometric data used to design the human model is generated from GEBOD, an anthropometric data regression software [6]. The third (q_3) , fourth (q_4) , and seventh (q_7) DOFs coincide, which means these three joints are located in the same place. The DOFs are presented in the local z-direction, and the local coordinates are set up at the end of each joint according to the DH method [10]. The global coordinates are considered as the parent branch in this 2D model, and it is divided into two child branches—the spine-arm branch and the leg branch. The two arms are combined into one since this is a 2D approximation, and the same combination is done for the two legs. Figure 1 illustrates the complete schematic of a 2D human model setup with DH coordinates. The model is based on a subject who is 1.763 meters tall and weighs 83.737 kilograms. The detailed anthropometric information about the biomechanical model is provided in Table 2.

The DH method is used to derive the kinematic equations for the 2D model. This method is especially useful for transferring the local coordinates to global coordinates through transformation matrices. The four DH parameters are θ , d, a, and α -where θ represents rotation angle along the previous z axis, d represents the offset distance along the previous z axis, a represents the offset distance along the current x axis, and α represents rotation along the current x axis. Equation (1) gives the DH transformation matrix. Table 1 shows the DH table



Table 1 DH table for 2D human model					
DOF	θ	d	a	α	Segment
(+ dir)		(length of)	(length of)		(branch)
q_1 (global forward translation)	π	0	0	$\frac{\pi}{2}$	Global
q_2 (global upward translation)	$\frac{\pi}{2}$	Leg	0	$-\frac{\pi}{2}$	Global
q_3 (global clockwise rotation)	0	0	0	0	Global
q_4 (spine flexion)	$-\frac{\pi}{2}$	0	Spine	0	Spine arm
q_5 (shoulder flexion)	π	0	Upper arm	0	Spine arm
q_6 (elbow extension)	0	0	Lower arm	0	Spine arm
q_7 (hip extension)	$\frac{\pi}{2}$	0	Thigh	0	Leg
q_8 (knee flexion)	0	0	Tibia	0	Leg
q_9 (ankle plantar flexion)	$-\frac{\pi}{2}$	0	Hind foot	0	Leg
q_{10} (metatarsophalangeal extension)	0	0	Fore foot	0	Leg

Table 1 DH table for 2D human model

 Table 2
 Anthropometric data for 2D human model

Link index (i)	Length (m)	Mass (kg)	COM ^d (m)	Inertia ^c (kgm ²)
1 (Virtual link)	0	0	0	$\mathbf{I}_{xx} = 0, \mathbf{I}_{yy} = 0, \mathbf{I}_{zz} = 0$
2 (Virtual link)	0	0	0	$\mathbf{I}_{xx} = 0, \mathbf{I}_{yy} = 0, \mathbf{I}_{zz} = 0$
3 (Virtual link)	0	0	0	$\mathbf{I}_{xx} = 0, \mathbf{I}_{yy} = 0, \mathbf{I}_{zz} = 0$
4 (Spine ^a)	$L_i = 0.57$	45.447	(-0.183, 0, 0)	$\mathbf{I}_{xx} = 0, \mathbf{I}_{yy} = 4.073, \mathbf{I}_{zz} = 4.073$
5 (Humerus)	$L_2 = 0.339$	4.072	(-0.189, 0, 0)	$\mathbf{I}_{xx} = 0, \mathbf{I}_{yy} = 0.176, \mathbf{I}_{zz} = 0.176$
6 (Radius and Ulna)	$L_3 = 0.311$	3.877	(-0.173, 0, 0)	$\mathbf{I}_{xx} = 0, \mathbf{I}_{yy} = 0.135, \mathbf{I}_{zz} = 0.135$
7 (Femur ^b)	$L_4 = 0.465$	20.350	(-0.239, 0, 0)	$\mathbf{I}_{xx} = 0, \mathbf{I}_{yy} = 1.530, \mathbf{I}_{zz} = 1.530$
8 (Tibia and Fibula)	$L_5 = 0.433$	7.988	(-0.212, 0, 0)	$\mathbf{I}_{xx} = 0, \mathbf{I}_{yy} = 0.494, \mathbf{I}_{zz} = 0.494$
9 (Metatarsals)	$L_6 = 0.20$	1.794	(-0.145, 0, 0)	$\mathbf{I}_{xx} = 0, \mathbf{I}_{yy} = 0.081, \mathbf{I}_{zz} = 0.081$
10 (Phalanges)	$L_7 = 0.05$	0.199	(-0.025, 0, 0)	$\mathbf{I}_{xx} = 0, \mathbf{I}_{yy} = 0.009, \mathbf{I}_{zz} = 0.009$

^aNote that Mass, COM, and inertia of spine include neck and head.

for the 2D human model.

$$^{i-1}\mathbf{T}_{i} = \begin{bmatrix} \cos\theta_{i} & -\cos\alpha_{i}\sin\theta_{i} & \sin\alpha_{i}\sin\theta_{i} & a_{i}\cos\theta_{i} \\ \sin\theta_{i} & \cos\alpha_{i}\cos\theta_{i} & -\sin\alpha_{i}\cos\theta_{i} & a_{i}\sin\theta_{i} \\ 0 & \sin\theta_{i} & \cos\alpha_{i} & d_{i} \\ 0 & 0 & 0 & 1 \end{bmatrix}$$
(1)

where the top-left 3×3 submatrix represents the rotation matrix, and the top-right 3×1 represents the translation vector.



^bMass, COM, and inertia of femur include the pelvis.

^cExcept for spine link, other links combine the right and left limbs in sagittal plane. In addition, the inertia terms $\mathbf{I}_{xy} = \mathbf{I}_{xz} = \mathbf{I}_{yz} = 0$.

^dCOM and inertia are measured in DH local coordinates from the end of each link

3 Equations of motion and fatigue formulation

The recursive approach is used to calculate the kinematics and dynamics of the human model for this box-carrying task. Then, a simple three-compartment controller fatigue model is used to predict the maximum endurance time and progression of fatigue.

3.1 Equations of motion

The EOM are expressed in Eqs. (2)-(6), where the first term in the torque expression of Eq. (2) is the torque due to inertia and Coriolis force, the second term is the torque due to gravity force, the third term is the torque due to external force, and the fourth term represents the torque due to the external moment.

$$\tau_{i} = tr(\frac{\partial \mathbf{A}_{i}}{\partial q_{i}}\mathbf{D}_{i}) - \mathbf{g}^{T}\frac{\partial \mathbf{A}_{i}}{\partial q_{i}}\mathbf{E}_{i} - \mathbf{f}_{k}^{T}\frac{\partial \mathbf{A}_{i}}{\partial q_{i}}\mathbf{F}_{i} - \mathbf{G}_{k}^{T}\mathbf{A}_{i-1}\mathbf{z}_{0}$$
(2)

$$\mathbf{D}_{i} = \mathbf{I}_{i} \mathbf{C}_{i}^{\mathrm{T}} + \mathbf{T}_{i+1} \mathbf{D}_{i+1} \tag{3}$$

$$\mathbf{E}_{i} = m_{i}\mathbf{r}_{i} + \mathbf{T}_{i+1}\mathbf{E}_{i+1} \tag{4}$$

$$\mathbf{F}_{i} = \mathbf{r}_{k} \delta_{ki} + \mathbf{T}_{i+1} \mathbf{F}_{i+1} \tag{5}$$

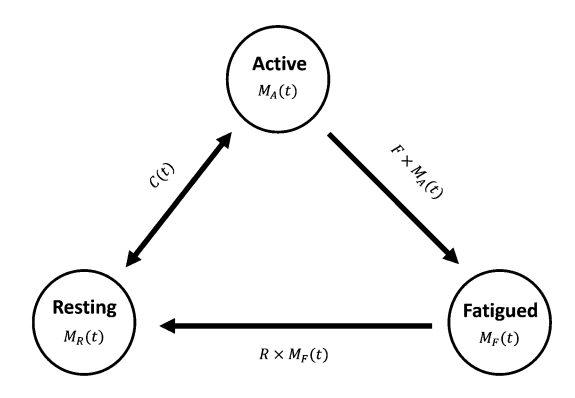
$$\mathbf{G}_{i} = \mathbf{h}_{k} \delta_{ki} + \mathbf{G}_{i+1} \tag{6}$$

where $tr(\cdot)$ is the trace of a matrix, $\mathbf{A_i}$ and $\mathbf{C_i}$ are the recursive kinematics position and acceleration matrices, respectively, q_i is the i-th joint angle, $\mathbf{I_i}$ is the inertia matrix for link i as defined in Eq. (7a), $\mathbf{D_i}$ is the recursive inertia and Coriolis matrix, \mathbf{g} is the gravity vector, m_i is the mass of link i, $\mathbf{r_i}$ is the center of mass of link i, $\mathbf{f_k} = \begin{bmatrix} 0 & f_{ky} & f_{kz} & 0 \end{bmatrix}^T$ is the external force applied on link k, $\mathbf{r_k}$ is the position of the external force in the local frame k, $\mathbf{h_k} = \begin{bmatrix} h_x & 0 & 0 & 0 \end{bmatrix}^T$ is the external moment applied on link k, $\mathbf{T_i}$ is the link transformation matrix, $\mathbf{z_0} = \begin{bmatrix} 0 & 0 & 1 & 0 \end{bmatrix}^T$ for a revolute joint, $\mathbf{z_0} = \begin{bmatrix} 0 & 0 & 0 & 0 \end{bmatrix}^T$ for a prismatic joint, and δ_{ki} is the Kronecker delta defined in Eq. (7b). For a detailed derivation of the EOM and their sensitivities with respect to state variables, refer to Xiang et al. [29]. A force balance foot-ground interaction model is used to calculate ground reaction forces (GRF), which equals to the active forces acting on the body, including inertia and Coriolis force, gravity, and external box weight. This active-passive (GRF) balance model was presented in Xiang et al. [30] and Xiang et al. [31]. By applying this contact model, the global forces/torque will become zero if the balance condition is satisfied in optimization.

$$\mathbf{I}_{i} = \begin{bmatrix} \frac{-I_{xx} + I_{yy} + I_{zz}}{2} & I_{xy} & I_{xz} & m_{i} x_{i_{COM}} \\ I_{xy} & \frac{I_{xx} - I_{yy} + I_{zz}}{2} & I_{yz} & m_{i} y_{i_{COM}} \\ I_{xz} & I_{yz} & \frac{I_{xx} + I_{yy} - I_{zz}}{2} & m_{i} z_{i_{COM}} \\ m_{i} x_{i_{COM}} & m_{i} y_{i_{COM}} & m_{i} z_{i_{COM}} & m_{i} \end{bmatrix}$$
(7a)

$$\delta_{ki} = \begin{cases} 1 & \text{when } k = i \\ 0 & \text{otherwise} \end{cases}$$
 (7b)

Fig. 2 Three-compartment fatigue model with workflow [27]



3.2 Fatigue formulation

The three-compartment controller fatigue model has three basic elements – resting, active, and fatigued compartments. Figure 2 shows the schematic of this system and the flow between the compartments, which is governed mathematically by the three first-order differential equations as in Eqs. (8)-(10). A relative unit-less measure of joint torque in percent of maximum torque (%strength) is used in these equations.

$$\frac{\mathrm{d}M_{\mathrm{Ri}}(t)}{\mathrm{d}t} = -C_{\mathrm{i}}(t) + R_{\mathrm{i}} \times M_{\mathrm{Fi}}(t) \tag{8}$$

$$\frac{\mathrm{d}M_{\mathrm{Ai}}(t)}{\mathrm{d}t} = C_{\mathrm{i}}(t) - F_{\mathrm{i}} \times M_{\mathrm{Ai}}(t) \tag{9}$$

$$\frac{\mathrm{d}M_{\mathrm{Fi}}(t)}{\mathrm{d}t} = F_{\mathrm{i}} \times M_{\mathrm{Ai}}(t) - R_{\mathrm{i}} \times M_{\mathrm{Fi}}(t) \tag{10}$$

where $M_{Ai}(t)$ is the active joint torque for the i-th joint at time instant t, $M_{Fi}(t)$ is the fatigued joint torque for the i-th joint at time instant t, $M_{Ri}(t)$ is the resting joint torque for the i-th joint at time instant t, R_i is the recovery coefficient for the i-th joint, F_i is fatigue coefficient for the i-th joint, and $C_i(t)$ is a bidirectional, time-varying torque activation—deactivation drive for the i-th joint at time instant t, which relates $M_{Ai}(t)$ and $M_{Ri}(t)$. The fatigue and recovery coefficient values [9] for all five physical joints are reported in Table 3. The hip joint is excluded from the study as the respective coefficients are not available in the aforementioned article. The values of $C_i(t)$ satisfy the conditions given by Eqs. (11)-(13).

If
$$M_{Ai}(t) < TL_i(t)$$
 and $M_{Ri}(t) > TL_i(t) - M_{Ai}(t)$, $C_i(t) = L_{Di} \times [TL_i(t) - M_{Ai}(t)]$ (11)

If
$$M_{Ai}(t) < TL_i(t)$$
 and $M_{Ri}(t) < TL_i(t) - M_{Ai}(t)$, $C_i(t) = L_{Di} \times M_{Ri}(t)$ (12)

If
$$M_{Ai}(t) \ge TL_i(t), \ C_i(t) = L_{Ri} \times [TL_i(t) - M_{Ai}(t)]$$
 (13)

where $L_{\rm Di}$ denotes the force development factor, and $L_{\rm Ri}$ denotes the relaxation factor. Varying the values of $L_{\rm Di}$ and $L_{\rm Ri}$ by 2500% alters endurance time by only 10%, so arbitrary values consistent with literature [9] are assigned for these parameters, i.e., $L_{\rm Di} = 10$ and $L_{\rm Ri} = 10$. $TL_{\rm i}(t)$ represents the target load for each joint at time instant t, which is calculated



Table 3	Fatigue and Recove	ry
Coefficie	ents [9]	

DOF	F	R
Spine (q_4)	0.00755	0.00075
Shoulder (q_5)	0.01820	0.00168
Elbow (q_6)	0.00912	0.00094
Knee (q_8)	0.01500	0.00149
Ankle (q_9)	0.00589	0.00058

using Eq. (14).

$$TL_{i}(t) = \begin{cases} \frac{\tau_{i}(t)}{\tau_{i}^{U}} & \text{for + ve torque direction} \\ \frac{\tau_{i}(t)}{\tau_{i}^{L}} & \text{for - ve torque direction} \end{cases}$$
 (14)

4 Optimization formulation

In this section, the elements of the constrained optimization formulation, i.e., the objective function, the design variables and their initial guess, and the constraints are discussed.

4.1 Objective function

The endurance time for the box carrying-fatigue problem could be stated as the maximum time (Eq. (15)) the carrying task can be sustained before muscle fatigue contributes to its failure.

Maximize:
$$T$$
 (15)

where T is the endurance time.

4.2 Design variables

Design variables are the entities that can change their values within a specified range during the optimization process. Since the optimization is carried out in joint space, the joint angles \mathbf{q} (Eq. (16)) are considered a part of the design variables set.

$$\mathbf{q} = \begin{bmatrix} q_1 & q_2 & q_3 & \dots & q_{\text{ndof}} \end{bmatrix}^{\text{T}} \tag{16}$$

From the three-compartment controller fatigue model [27], the resting compartment $M_{Ri}(t)$, the active compartment $M_{Ai}(t)$, and the fatigued compartment $M_{Fi}(t)$ are considered design variables. These time-dependent parameters are transformed from a continuous-time domain to a discrete-time domain. Spline interpolation is used to get an interpolation formula that is continuous in both the first and second derivatives within the intervals and at the interpolating nodes. This is a necessary condition for the optimization task. The design variables are parameterized using cubic B-splines as given by Eqs. (17)-(19).

$$M_{\rm Ri}(t) = \sum_{\rm j=1}^{\rm m} B_{\rm j}(t) P_{\rm M_{\rm Rij}}$$
 (17)



$$M_{Ai}(t) = \sum_{i=1}^{m} B_{j}(t) P_{M_{Aij}}$$
 (18)

$$M_{\rm Fi}(t) = \sum_{\rm i=1}^{\rm m} B_{\rm j}(t) P_{\rm M_{\rm Fij}}$$
 (19)

where the subscript i ϵ 4, 5, 6, 8, 9 denotes the corresponding DOF.

 $P_{\rm M_{Rij}}$, $P_{\rm M_{Aij}}$, and $P_{\rm M_{Fij}}$ denote the control points of the resting, active, and fatigued compartments, respectively. Equations (20)-(22) denote the control point vectors for the three compartments. With this representation, the control points become the design variables for the parameterized optimization problem. The design variables associated with the three compartments can then be represented by these control point vectors.

$$\mathbf{P}_{\mathbf{M}_{\mathrm{Ri}}} = \begin{bmatrix} P_{\mathbf{M}_{\mathrm{Ri1}}} & P_{\mathbf{M}_{\mathrm{Ri2}}} & P_{\mathbf{M}_{\mathrm{Ri3}}} & \dots & P_{\mathbf{M}_{\mathrm{Rim}}} \end{bmatrix}^{\mathrm{T}}$$
 (20)

$$\mathbf{P}_{\mathbf{M}_{\mathrm{Ai}}} = \begin{bmatrix} P_{\mathbf{M}_{\mathrm{Ai1}}} & P_{\mathbf{M}_{\mathrm{Ai2}}} & P_{\mathbf{M}_{\mathrm{Ai3}}} & \dots & P_{\mathbf{M}_{\mathrm{Aim}}} \end{bmatrix}^{\mathrm{T}}$$
 (21)

$$\mathbf{P}_{\mathbf{M}_{\mathrm{Fi}}} = \begin{bmatrix} P_{\mathbf{M}_{\mathrm{Fi}1}} & P_{\mathbf{M}_{\mathrm{Fi}2}} & P_{\mathbf{M}_{\mathrm{Fi}3}} & \dots & P_{\mathbf{M}_{\mathrm{Fim}}} \end{bmatrix}^{\mathrm{T}}$$
 (22)

where m is the total number of control points.

 $B_{\rm j}(t)$ is the basis function at time instant t. The B-spline basis functions are uniquely determined by a knot vector \mathbf{t} , which is evenly spaced on the time interval $\begin{bmatrix} 0 & T \end{bmatrix}^{\rm T}$ with the time step Δt , as shown in Eqs. (23)-(24).

$$\mathbf{t} = \begin{bmatrix} t_0 & t_1 & t_2 & \dots & t_{s-1} \end{bmatrix}^{\mathrm{T}}$$
 (23)

$$t_{k+1} = t_k + \Delta t, \quad \Delta t = \frac{T}{s}, \quad k = 0, \dots, s-1$$
 (24)

where s is the number of discretized grids.

The number of knots depends on the number of control points and B-spline degree (nknot=nctrl+deg-1). More control points will generate more flexible curve but will increase the computational cost since they are design variables. To get the appropriate number of control points, some numerical tests are required. In this study, we used 13 control points for each cubic B-spline so that the number of knots is $13(nctrl) + 3(cubic\ deg) - 1 = 15$. The total time T is also considered as a design variable and discretized into 11 uniform grid points with a time step of T/10. This led to a total number of 206 (ndof+3*5*nctrl+1) design variables. All parts of the design variable set can now be accumulated and represented by Eq. (25).

$$\mathbf{x} = \begin{bmatrix} \mathbf{q}^{\mathrm{T}} & \mathbf{P}_{\mathrm{M}_{\mathrm{R}i}}^{\mathrm{T}} & \mathbf{P}_{\mathrm{M}_{\mathrm{A}i}}^{\mathrm{T}} & \mathbf{P}_{\mathrm{M}_{\mathrm{F}i}}^{\mathrm{T}} & T \end{bmatrix}^{\mathrm{T}}$$
(25)

The initial guess of the joint angles and fatigued compartments are set to zero, but the active compartment value is set to 0.6 and the resting compartment value is set to 0.4, showing the fact that the optimization process starts when joints have active torques. The endurance time is estimated as 10 seconds initially. The optimization problem is solved using the SNOPT program, which uses a SQP algorithm algorithm [12]. The constraints imposed upon the optimization formulation are discussed in the next section.



140.0

60.0

0.0

T11 4 T1 . 4 1 T1 .			
Table 4 Joint Angle Limits	DOF	Lower limit	Upper limit
	q_1 (m)	-5.0	5.0
	q_2 (m)	-5.0	5.0
	q_3 (deg)	-10.0	10.0
	q_4 (deg)	0.0	120.0
	q_5 (deg)	-180.0	90.0
	q_6 (deg)	-150.0	0.0
	q_7 (deg)	-150.0	90.0

0.0

-20.0

-60.0

 q_8 (deg)

 q_0 (deg)

 q_{10} (deg)

4.3 Constraints

Both time-dependent and time-independent constraints are considered in the box carrying-fatigue optimization formulation. For the entire time interval, time-dependent constraints such as joint angle limits, joint torque limits, foot contacting position, zero-moment point (ZMP) location, wrist location for the box weight, resting compartment equation, active compartment equation, and fatigued compartment are considered. In addition, the three compartments must satisfy the unit summation condition $[M_{Ai}(t) + M_{Ri}(t) + M_{Fi}(t) = 1]$ and residual capacity condition $[M_{Ai}(t) + M_{Ri}(t) \ge TL_i(t)]$. For the time-independent constraints, the lower body (hip, knee, and ankle joints) is in a straight posture. Finally, the failure condition for a joint is defined as the sum of active and resting joint torques dropping below the target load value. Therefore, the task is considered to fail when one joint fails or multiple joints fail simultaneously. This is described by a coupled failure constraint, which is the multiplication of the five joint failure conditions – spine, shoulder, elbow, knee, and ankle at the final time point. By specifying a small tolerance for the task failure constraint, it is forced to be active at the final time instant. After the optimal solution is found, this coupled failure constraint can be used to check which joint fails first.

Time dependent constraints

4.3.1 Joint limits

An upper and lower limit was set for all the joint angles to ensure the optimizer varies these design variables within a physical range.

$$q_{\rm i}^{\rm L} \le q_{\rm i}(\mathbf{x}) \le q_{\rm i}^{\rm U} \tag{26}$$

where $q_{\rm i}^{\rm L}$ is the lower limit and $q_{\rm i}^{\rm U}$ is the upper limit. These values are reported in Table 4.

4.3.2 Torque limits

Normalized torque limits were set to ensure the physical torque achieved from the EOM does not exceed the strength limit during the box carrying-fatigue optimization process.

$$0 \le \frac{\tau_i(\mathbf{x}) - \tau_i^L}{\tau_i^U - \tau_i^L} \le 1 \tag{27}$$



Table 5 Joint Torque Limits [4, 15, 16, 32]	DOF	Lower limit	Upper limit
	q_1 (N)	-500.0	500.0
	$q_2(N)$	-500.0	500.0
	q ₃ (Nm)	-500.0	500.0
Note that the strengths of $q_5 - q_{10}$ are doubled because of	q4 (Nm)	-400.0	400.0
the combination of the right and left limbs' strengths in 2D model.	q ₅ (Nm)	-184.0	126.0
	q ₆ (Nm)	-117.4	120.6
In addition, the global	q ₇ (Nm)	-334.0	408.0
forces/torque are becoming zero after applying the foot-GRF	q_8 (Nm)	-518.2	206.4
balance interaction model	$q_{\rm Q}$ (Nm)	-75.4	170.6
although large bounds are used for global forces/torque	q ₁₀ (Nm)	-140.0	140.0

where τ_i^L is the lower limit and τ_i^U is the upper limit of the i-th joint torque. This constraint is applied to all the joints. These values are reported in Table 5.

4.3.3 Foot contact position

The position where the feet contact the ground is also specified in order to prevent feet of the human model from leaving the ground. The specific position depends on the length of the foot, which varies for each subject. The heel (z = -0.05 m), ankle (z = 0.0 m) and the toe (z = 0.20 m) are given and the feet length 0.25 m.

$$\mathbf{P}_{\text{feet}}(\mathbf{x}) = \mathbf{P}_{\text{feet}}^{\text{specified}} \tag{28}$$

where $\mathbf{P}_{\text{feet}}^{\text{specified}}$ is the specified foot contact position on level ground.

4.3.4 Zero-moment point

The zero-moment point should always stay inside the foot support polygon (FSP). For the 2D model, the FSP becomes a line segment that only has z coordinates in the sagittal plane in global Cartesian coordinates. The z-coordinate of ZMP is between the heel and toe, which are fixed on the ground.

$$\mathbf{P}_{\mathsf{ZMP}}(\mathbf{x}) \in \mathsf{FSP}$$
 (29)

4.3.5 Wrist location

The wrist location corresponding to the box position is specified as (0, 1.05, 0.4) m.

$$\mathbf{P}_{\text{wrist}}(\mathbf{x}) = \mathbf{P}_{\text{wrist}}^{\text{specified}} \tag{30}$$

4.3.6 Governing equations for three motor unit compartments

The three compartments must satisfy the governing Eqs. (31)-(33):

$$\frac{\mathrm{d}M_{\mathrm{Ri}}(t)}{\mathrm{d}t} + C_{\mathrm{i}}(t) - R_{\mathrm{i}} \times M_{\mathrm{Fi}}(t) = 0 \tag{31}$$



$$\frac{dM_{Ai}(t)}{dt} - C_{i}(t) + F_{i} \times M_{Ai}(t) = 0$$
(32)

$$\frac{\mathrm{d}M_{\mathrm{Fi}}(t)}{\mathrm{d}t} - F_{\mathrm{i}} \times M_{\mathrm{Ai}}(t) + R_{\mathrm{i}} \times M_{\mathrm{Fi}}(t) = 0 \tag{33}$$

These three constraints are applied to the five physical joints (spine, shoulder, elbow, knee, and ankle) only.

4.3.7 Unit summation

The sum of the values of three compartments at each instant must equal to one.

$$M_{\text{Ri}}(t) + M_{\text{Ai}}(t) + M_{\text{Fi}}(t) = 1$$
 (34)

This constraint is also applied to the five physical joints.

4.3.8 Residual capacity (RC)

The joint residual capacity should meet or exceed the target load for all five physical joints at all times.

$$M_{\rm Ri}(t) + M_{\rm Ai}(t) \ge TL_{\rm i}(t) \tag{35}$$

Time independent constraints

4.3.9 Lower body posture

The lower body (hip, knee, and ankle joints) posture was restricted to a narrow range of motion ($q_7^{\text{specified}} = -0.974 \text{ deg}$, $q_8^{\text{specified}} = 4.183 \text{ deg}$, and $q_9^{\text{specified}} = -3.209 \text{ deg}$) corresponding to mostly upright postures.

Hip:
$$-15^{\circ} < q_7 - q_7^{\text{specified}} < 15^{\circ}$$
 (36)

Knee:
$$-15^{\circ} < q_8 - q_8^{\text{specified}} < 15^{\circ}$$
 (37)

Ankle:
$$-15^{\circ} < q_9 - q_9^{\text{specified}} < 15^{\circ}$$
 (38)

4.3.10 Coupled failure condition

The five physical joints (spine, shoulder, elbow, knee, and ankle) were coupled together to determine which joints fatigue the earliest. This is achieved by multiplying the residual capacities of these joints.

$$-\epsilon < \prod_{i=4, i\neq 7}^{9} \left[M_{Ri}(T) + M_{Ai}(T) - TL_{i}(T) \right] < +\epsilon \tag{39}$$

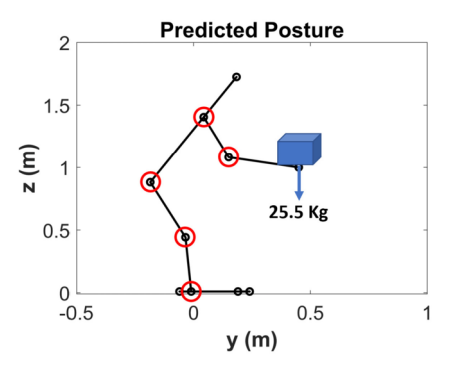
where ϵ denotes the tolerance limit, and its value is given by 10^{-5} .



Table 6 Optimized joint angles and torques

DOF	Angle	Torque
(+ dir)	(radians)	(Nm)
Spine (q_4)	0.587	-288.7
Shoulder (q_5)	-0.733	-133.0
Elbow (q_6)	-0.982	-95.0
Knee (q_8)	0.273	149.1
Ankle (q_9)	0.057	123.1

Fig. 3 Predicted posture for carrying-fatigue optimization problem (The fatigue models are considered for the joints circled in red). (Color figure online)



4.3.11 Initial conditions for the three compartments

The five physical joints are fully activated at the initial time.

$$M_{\rm Ai}(0) = 1.0$$
 (40)

$$M_{\rm Ri}(0) = 0.0 \tag{41}$$

$$M_{\rm Fi}(0) = 0.0$$
 (42)

5 Results and discussion

The inverse dynamics optimization method is utilized to predict the optimal box carrying posture, maximum endurance time, and joint fatigue progression for the subject who holds a 25.5 kg box. The optimal carrying posture is depicted in Fig. 3. Note that the feet are fixed to the ground, and the global location of the box is specified. The fatigue models are considered only for the joints circled in red. The optimized joint angles and torques are reported in Table 6. The maximum endurance time is 15.71 seconds. The optimization process takes 64 major iterations and 5.04 seconds of CPU time to converge. The simulation is run on a laptop with an 11th Gen Intel Core i9-11900H processor clocked at 2.50 GHz base speed, which features 8 cores, 16 logical processors and 32 GB RAM. The joint limits, foot contacting position, wrist position, and unit summation constraints are active during the optimization process.

From Figs. 4, 5, 6, 7 and 8 the differences between the target load and residual capacity values (failure conditions) at the maximum endurance time instant can be used to find out which joint fails first. The failure condition values are given in Table 7, which indicates that



Table 7 Joint failure conditions

DOF (+ dir)	Failure condition $[RC(T) - TL(T)]$
Elbow (q_6)	0.000000
Knee (q_8)	0.002203
Shoulder (q_5)	0.004255
Spine (q_4)	0.010907
Ankle (q_9)	0.030947

Fig. 4 Predicted compartment values for elbow joint. (Color figure online)

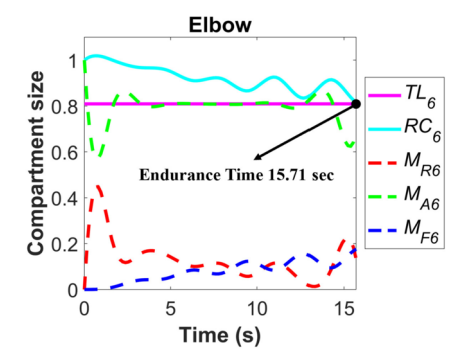
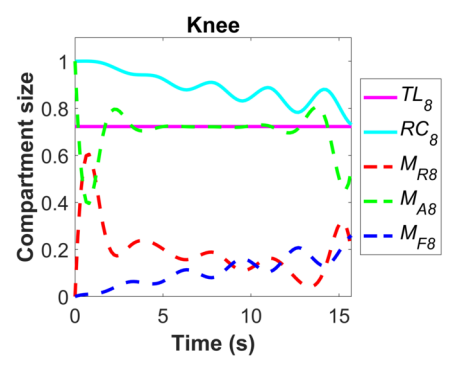


Fig. 5 Predicted compartment values for knee joint. (Color figure online)



the elbow joint fails first and the ankle joint fails last during the endurance test. The table also reveals that elbow and knee joints contribute to the bulk of the task, correctly predicting the nature of a typical carrying posture. The three-compartment values for the elbow, knee, shoulder, spine and ankle joints are also shown in Figs. 4-8. All five physical joints show a common trend of diminishing joint residual capacity and increasing fatigue over the entirety of the endurance test. The joint active torque, $M_{Ai}(t)$ quickly falls to a certain value (40% of its maximum value for shoulder, knee, spine and ankle joints, 60% of its maximum value for elbow joint) at 0.6 seconds, but partially recovers (to about 80% of the maximum value for the shoulder, knee, spine, and ankle joints, and to about 85% of the maximum value for the elbow joint) at 2.2 seconds and maintains a stable value around the target load value till fatigue is reached. The joint resting torques, $M_{Ri}(t)$ undergo a surge (to about 60% of its maximum value for the shoulder, knee, spine and ankle joints, and about 45% of its maximum value for the elbow joint) at 0.8 seconds before they fall to a certain value (about



Fig. 6 Predicted compartment values for shoulder joint. (Color figure online)

Shoulder

TL₅

RC₅

-- M_{R5}

-- M_{F5}

Time (s)

Fig. 7 Predicted compartment values for spine joint. (Color figure online)

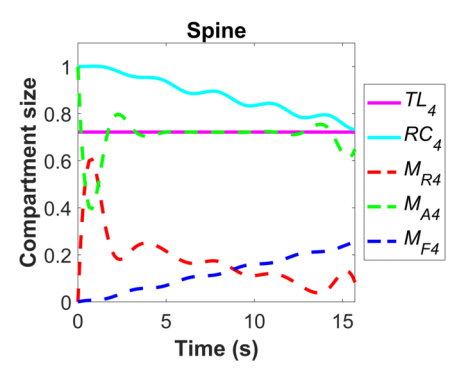
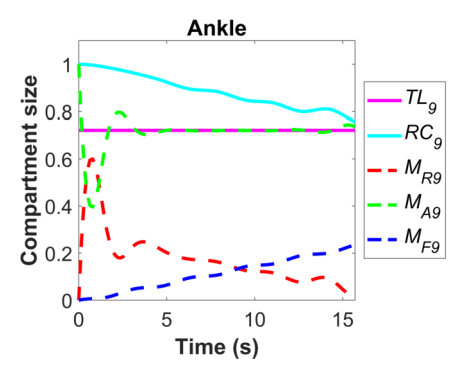


Fig. 8 Predicted compartment values for ankle joint. (Color figure online)



15% for the shoulder, knee, spine, and ankle joints, about 10% for the elbow joint) at 2.4 seconds, after which they have a slight rise before continuing to gradually decrease till task failed. This decrease is wavelike for all five physical joints. Fatigued joint torques, $M_{\rm Fi}(t)$ for all five physical joints gradually increase over time as expected. This increase is wavelike for shoulder, elbow, and knee joints but smooth for the other two (spine and ankle) physical joints. The target load stays about 72% of joint activation over the endurance time period for all five physical joints. The residual capacities decrease over the course of the endurance test for all five physical joints.

The exclusion of hip joint fatigue may change the results obtained in this study. One way to fix this would be to use the fatigue parameters for general joints as the parameters for hip



joint instead of specific hip fatigue parameters as suggested in Frey-Law et al. [9]. However, in general, for fatigue-based box carrying posture prediction, the upper body joints normally reach fatigue faster than the lower body joints. Therefore, we assume in this study that exclusion of hip joint fatigue will not significantly change the endurance time in standing up box carrying task. In addition, the proposed optimization formulation is generic, and the hip joint fatigue can be easily considered as long as its fatigue parameters are available. The experimental measurements of hip joint fatigue parameters are ongoing, and hip fatigue will be included in the future study.

For the box carrying task, we assume a straight standing lower body posture in constraint Eqs. (36)-(38). However, we did not specify the lower body joints to be the exact standing neutral angles that are close to zero [17]. Instead, a small range of motion (30°) is used for hip, knee, and ankle joints to allow the subject to adjust the lower body posture while keeping a relatively straight standing posture. This small lower body range of motion may improve the predicted endurance time. However, if the range of motion of the lower body is too large, optimization may predict an unnatural box carrying posture, such as knee bending posture. In addition, by using a gradient-based optimizer, it is possible to fall into a local optimum. In this study, we tried different starting points for design variables and took the maximum value of the predicted endurance time as the optimal solution to try to avoid a local optimum.

As $M_{Ai}(t)$ and $M_{Ri}(t)$ are both considered as part of design variables, they can vary throughout the optimization process if the governing equations of the three-compartment fatigue model are satisfied. For all joints, $M_{Ai}(t)$ is specified as 1(100%), and $M_{Ri}(t)$ and $M_{Fi}(t)$ are specified as 0(0%) at the initial time as in Eqs. (40)-(42). Based on Eq. (13), the bidirectional torque activation-deactivation drive $C_i(t)$ is negative at the beginning time because $TL_i(t) - M_{Ai}(t) < 0$, which means the extra $M_{Ai}(t)$ will flow into $M_{Ri}(t)$ as shown in Fig. 2. This will make $M_{Ai}(t)$ decrease and $M_{Ri}(t)$ increase as demonstrated in Figs. 4-8 for joint fatigue. When $M_{Ai}(t)$ keeps decreasing until it is below $TL_i(t)$, Eq. (11) is activated because $M_{Ai}(t) < TL_i(t)$ and $M_{Ri}(t) > [TL_i(t) - M_{Ai}(t)]$, and $C_i(t)$ is positive at this moment. Based on fatigue governing Eq. (9), although $C_i(t)$ is positive, $-F_i * M_{Ai}(t)$ is negative. Therefore, the derivative of $M_{Ai}(t)$ is still negative, i.e., $M_{Ai}(t)$ is still decreasing even $M_{Ai}(t) < TL_i(t)$ and $C_i(t) > 0$. The derivative of $M_{Ai}(t)$ is becoming positive until $C_i(t)$ is larger than $F_i * M_{Ai}(t)$. After that $M_{Ai}(t)$ starts to increase until it is greater than $TL_i(t)$ and sustains the $TL_i(t)$ together with $M_{Ri}(t)$. The minimum value of $M_{Ai}(t)$ and the maximum value of $M_{Ri}(t)$ occur at around 0.7 seconds.

In addition, in this study, we assume that five physical joints are fully activated at initial time. This may not match with human physiology. For heavy box carrying task, the human central nervous system (CNS) may activate some joints immediately but other joints later. However, this is an instinctive process for human, and learning and training can even change initial joint activation extent and sequence, such as athlete weight lifting training. However, for simulation, it is generally difficult to tell the activation status for all joints at the initial time. The simulation does not converge with inappropriate combination of initial joint activations. Global optimization method, such as genetic algorithm, can be used to study the effect of different combinations of initial joint activation conditions on the predicted endurance time to better understand human CNS and physiology. The developed method provides a tool to study this topic which is our future research.

In summary, the dynamic process of $M_{Ai}(t)$, $M_{Ri}(t)$ and $M_{Fi}(t)$ is governed by the fatigue governing differential Eqs. (8)-(10) and bidirectional control Eqs. (11)-(13) for $C_i(t)$. These equations are further controlled by the parameters R_i , F_i , L_{Ri} , and L_{Di} . Especially at the beginning stage (less than 0.7 seconds), $M_{Ai}(t)$ decreases below $TL_i(t)$, this is related to



the parameters $L_{\rm Ri}$ in Eq. (11) for $C_{\rm i}(t)$ and $F_{\rm i}$ in Eq. (9) for the derivative of $M_{\rm Ai}(t)$. $R_{\rm i}$ and $F_{\rm i}$ parameters are obtained from experiments. $L_{\rm Ri}$ and $L_{\rm Di}$ do not significantly affect the predicted endurance time based on Frey-Law et al. [9], but they do affect the dynamic behaviors of $M_{\rm Ai}(t)$ and $M_{\rm Ri}(t)$ at the beginning stage of the task as demonstrated in this study. This indicates $L_{\rm Ri}$ and $L_{\rm Di}$ are related to muscle physiology and are required further investigation.

6 Conclusion

The addition of the 3CC fatigue model with the existing inverse dynamics prediction technique enabled the determination of endurance time during box carrying-fatigue simulation. Not only can the optimized joint angles, joint torques, and ground reaction forces be obtained, the joint failure conditions can also be predicted along with the maximum endurance time. At the beginning of the task, active torque is high; then, as time progresses, the fatigue starts to occur until endurance time is reached, at which time muscle capacities fall below a threshold, and the task can no longer be continued. In the future, the static fatigue model will be extended to a dynamic fatigue model and integrated with motion prediction routines for analyzing fatigue effect and endurance time for repetitive lifting motion thus significantly improving the risk assessment tools for injury prevention during manual material handling processes.

Acknowledgements This work was supported by the National Science Foundation (CBET 2014281 and 2014278).

References

- Abbiss, C.R., Laursen, P.B.: Models to explain fatigue during prolonged endurance cycling. Sports Med. 35(10), 865–898 (2005)
- Barman, S., Xiang, Y.: Recursive Newton-Euler dynamics and sensitivity analysis for robot manipulator
 with revolute joints. In: International Design Engineering Technical Conferences and Computers and
 Information in Engineering Conference, Aug. 17-19, Virtual, Online (2020). https://doi.org/10.1115/ DETC2020-22646
- Barry, B.K., Enoka, R.M.: The neurobiology of muscle fatigue: 15 years later. Integr. Comp. Biol. 47(4), 465–473 (2007)
- Cahalan, T., Johnson, M., Liu, S., Chao, E.: Quantitative measurements of hip strength in different agegroups. Clin. Orthop. Relat. Res. R(246), 136–145 (1989)
- Charney, W., Zimmerman, K., Walara, E.: The lifting team. A design method to reduce lost time back injury in nursing. AAOHN J. 39(5), 231–234 (1991)
- Cheng, H., Obergefell, L., Rizer, A.: Generator of body (GEBOD) manual. AL/CF-TR-1994-0051, Armstrong Laboratory, Air Force Materiel Command. Wright-Patterson Air Force Base, Ohio (1994)
- Daynard, D., Yassi, A., Cooper, J., Tate, R., Norman, R., Wells, R.: Biomechanical analysis of peak and cumulative spinal loads during simulated patient-handling activities: a substudy of a randomized controlled trial to prevent lift and transfer injury of health care workers. Appl. Ergon. 32(3), 199–214 (2001)
- 8. Fitts, R.H.: Cellular mechanisms of muscle fatigue. Physiol. Rev. 74(1), 49–94 (1994)
- Frey-Law, L.A., Looft, J.M., Heitsman, J.: A three-compartment muscle fatigue model accurately predicts joint-specific maximum endurance times for sustained isometric tasks. J. Biomech. 45(10), 1803–1808 (2012)
- Fu, K.S., Gonzalez, R., Lee, C.: Robotics: Control, Sensing, Vision, and Intelligence. McGraw-Hill, New York (1987)
- Giat, Y., Mizrahi, J., Levy, M.: A musculotendon model of the fatigue profiles of paralyzed quadriceps muscle under FES. IEEE Trans. Biomed. Eng. 40(7), 664–674 (1993)



- Gill, P.E., Murray, W., Saunders, M.A.: SNOPT: an SQP algorithm for large-scale constrained optimization. J. Soc. Ind. Appl. Math. 47(1), 99–131 (2005)
- Hawkins, D., Hull, M.L.: Muscle force as affected by fatigue: mathematical model and experimental verification. J. Biomech. 26(9), 1117–1128 (1993)
- Howard, B., Cloutier, A., Yang, J.: Physics-based seated posture prediction for pregnant women and validation considering ground and seat pan contacts. J. Biomech. Eng. 134(7), 071004 (2012)
- Kaminski, T., Perrin, D., Gansneder, B.: Eversion strength analysis of uninjured and functionally unstable ankles. J. Athl. Train. 34(3), 239–245 (1999)
- Kumar, S.: Isolated planar trunk strengths measurement in normals. 3. Results and database. Int. J. Ind. Ergon. 17(2), 103–111 (1996)
- 17. Kwon, H.J., Chung, H.J., Xiang, Y.: Human gait prediction with a high dof upper body: a multi-objective optimization of discomfort and energy cost. Int. J. Humanoid Robot. 14(1), 1650025 (2017)
- Ma, L., Chablat, D., Bennis, F., Zhang, W.: A new simple dynamic muscle fatigue model and its validation. Int. J. Ind. Ergon. 39(1), 211–220 (2009)
- Marler, R.T., Arora, J.S.: Survey of multi-objective optimization methods for engineering. Struct. Multidiscip. Optim. 26(6), 369–395 (2004)
- Marras, W.S., Davis, K.G., Kirking, B.C., Granata, K.P.: Spine loading and trunk kinematics during team lifting. Ergonomics 42(10), 1258–1273 (1999)
- Pereira, A.F., Silva, M.T., Martins, J.M., de Carvalho, M.: Implementation of an efficient muscle fatigue model in the framework of multibody systems dynamics for analysis of human movements. J. Multi-Body Dyn. 225(4), 359–370 (2011)
- Peternel, L., Fang, C., Tsagarakis, N., Ajoudani, A.: A selective muscle fatigue management approach to ergonomic human-robot co-manipulation. Robot. Comput.-Integr. Manuf. 58, 69–79 (2019)
- Reed, M.P., Manary, M.A., Flannagan, C.A.C., Schneider, L.W.: A statistical method for predicting automobile driving posture. Hum. Factors 44(4), 557–568 (2002)
- Rohmert, W.: Determination of recovery pause for static work of man. Int. Z. Angew. Physiol. Einschl. Arbeitsphysiol. 18, 123–164 (1960)
- Song, J., Qu, X., Chen, C.-H.: Simulation of lifting motions using a novel multi-objective optimization approach. Int. J. Ind. Ergon. 53(100), 37–47 (2016)
- Wang, X.: A behavior-based inverse kinematics algorithm to predict arm prehension postures for computer-aided ergonomic evaluation. J. Biomech. 32(5), 453–460 (1999)
- Xia, T., Frey Law, L.A.: A theoretical approach for modeling peripheral muscle fatigue and recovery. J. Biomech. 41(14), 3046–3052 (2008)
- 28. Xiang, Y., Arefeen, A.: Two-dimensional team lifting prediction with floating-base box dynamics and grasping force coupling. Multibody Syst. Dyn. **50**(2), 211–231 (2020)
- Xiang, Y., Arora, J., Abdel-Malek, K.: Optimization-based motion prediction of mechanical systems: sensitivity analysis. Struct. Multidiscip. Optim. 37, 595–608 (2009)
- Xiang, Y., Arora, J., Rahmatalla, S., Abdel-Malek, K.: Optimization-based dynamic human walking prediction: one step formulation. Int. J. Numer. Methods Eng. 76(6), 667–695 (2009)
- Xiang, Y., Arora, J., Rahmatalla, S., Marler, R., Bhatt, R., Abdel-Malek, K.: Human lifting simulation using a multi-objective optimization approach. Multibody Syst. Dyn. 23, 431–451 (2010)
- Xiang, Y., Arora, J., chung, H., Kwon, H., Rahmatalla, S., Bhatt, R., Abdel-Malek, K.: Predictive simulation of human walking transitions using an optimization formulation. Struct. Multidiscip. Optim. 45(5), 759–772 (2012)
- Yang, J., Marler, R.T., Kim, H., Arora, J., Abdel-Malek, K.: Multi-objective optimization for upper body posture prediction. In: 10th AIAA/ISSMO Multidisciplinary Analysis and Optimization Conference, Aug. 30 - Sep. 1, Albany, New York (2004). https://doi.org/10.2514/6.2004-4506.
- Yang, J., Marler, T., Rahmatalla, S.: Multi-objective optimization-based method for kinematic posture prediction: development and validation. Robotica 29(2), 245–253 (2011)

Publisher's Note Springer Nature remains neutral with regard to jurisdictional claims in published maps and institutional affiliations.

